Sensitivity Studies of the Importance of Dust Ice Nuclei for the Indirect Aerosol Effect on Stratiform Mixed-Phase Clouds

U. LOHMANN

Institute for Atmospheric and Climate Science, ETH Zurich, Zurich, Switzerland

K. DIEHL

Institute for Atmospheric Physics, University of Mainz, Mainz, Germany

(Manuscript received 26 October 2004, in final form 21 July 2005)

ABSTRACT

New parameterizations of contact freezing and immersion freezing in stratiform mixed-phase clouds (with temperatures between 0° and −35°C) for black carbon and mineral dust assumed to be composed of either kaolinite (simulation KAO) or montmorillonite (simulation MON) are introduced into the ECHAM4 general circulation model. The effectiveness of black carbon and dust as ice nuclei as a function of temperature is parameterized from a compilation of laboratory studies. This is the first time that freezing parameterizations take the chemical composition of ice nuclei into account. The rather subtle differences between these sensitivity simulations in the present-day climate have significant implications for the anthropogenic indirect aerosol effect. The decrease in net radiation in these sensitivity simulations at the top of the atmosphere varies from 1 ± 0.3 to 2.1 ± 0.1 W m^{-2} depending on whether dust is assumed to be composed of kaolinite or montmorillonite. In simulation KAO, black carbon has a higher relevancy as an ice nucleus than in simulation MON, because kaolinite is not freezing as effectively as montmorillonite. In simulation KAO, the addition of anthropogenic aerosols results in a larger ice water path, a slightly higher precipitation rate, and a reduced total cloud cover. On the contrary, in simulation MON the increase in ice water path is much smaller and globally the decrease in precipitation is dominated by the reduction in warm-phase precipitation due to the indirect cloud lifetime effect.

1. Introduction

Anthropogenic aerosol particles such as sulfate and carbonaceous (black carbon and organic carbon) aerosols have substantially increased the global mean burden of aerosol particles from preindustrial times to the present day. Aerosol particles affect the climate system via the following physical mechanisms: First, they can scatter and absorb solar radiation. Second, they can scatter, absorb, and emit thermal radiation. Third, aerosol particles act as cloud condensation nuclei (CCN) and ice nuclei (IN). The increase in cloud droplet number for a given cloud water content increases the cloud albedo (Twomey effect or aerosol cloud albedo effect). In addition, the precipitation efficiency of warm clouds is reduced, increasing cloud lifetime (aerosol cloud lifetime effect). Both effects are uncertain (Ramaswamy et al. 2001). They are estimated to have reduced the net radiation at the top of the atmosphere between 0 and −2 W m^{-2} (Lohmann and Lesins 2002; Anderson et al. 2003).

The influence of aerosol particles on changing the properties of ice forming nuclei is poorly understood because of the variety of heterogeneous ice crystal nucleation modes. Aerosols can act as IN by coming into contact with supercooled cloud droplets (contact freezing), or by initiating freezing from within a cloud droplet by immersion or condensation freezing, or by acting as deposition nuclei. Ice nuclei that initiate freezing are also referred to as freezing nuclei. Contact nucleation is usually the most efficient process at slight supercoolings, while at lower temperatures immersion freezing can be more prevalent as will be discussed in more detail below. Condensation and immersion freezing are difficult to separate. It is possible in experimental studies, and there generally similar freezing temperatures are found. For instance, Diehl et al. (2001, 2002) obtained a freezing onset temperature for pollen

Corresponding author address: Ulrike Lohmann, Institute for Atmospheric and Climate Science, ETH Zurich, Universitätsstr. 16, 8092 Zurich, Switzerland.
E-mail: ulrike.lohmann@env.ethz.ch

of −8°C in the condensation mode, and of −9°C in the immersion mode. Schaller and Fukuta (1979) obtained a freezing onset temperature for kaolinite of −10°C in the condensation mode to be compared to −14°C in the immersion mode (Pitter and Pruppacher 1973). Thus, immersion freezing will serve as a surrogate for both condensation and immersion freezing in this study. Deposition freezing generally takes place at lower temperatures than the other heterogeneous freezing processes. For example, Schaller and Fukuta (1979) obtained an onset temperature of −19°C in deposition mode at a 20% supersaturation with respect to ice. At lower supersaturations, the onset temperature is even lower. Therefore, depositional growth is neglected in this study. Unlike CCN, ice nuclei are generally insoluble particles, such as certain mineral dusts, soot, or black carbon, as well as some biological materials (see, e.g., Pitter and Pruppacher 1973; Levin and Yankofsky 1983; Diehl et al. 2001; Gorbunov et al. 2001).

Black carbon as a climate forcing agent has been studied extensively lately. It affects climate by absorbing solar radiation (Jacobson 2001) and significantly reducing the solar radiation reaching the surface (Ramanathan et al. 2001; Lohmann and Feichter 2001). The net reduction in shortwave radiation at the surface from all aerosol direct and indirect effects is estimated to be between −1.8 and −4 W m^{-2} (Lohmann and Feichter 2005). This will change the atmospheric stability and can have influences for convective activity and precipitation, especially over China and India (Menon et al. 2002). It was suggested that the reduction of black carbon maybe more important than that of greenhouse gases in terms of eliminating some of the anthropogenically induced climate change (Jacobson 2002). Here we evaluate its role as an ice nucleus.

Based on laboratory measurements by Gorbunov et al. (2001) that yield evidence for hydrophilic soot as contact ice nuclei, Lohmann (2002a) investigated the effectiveness of black carbon as a contact ice nucleus. She hypothesized that if a fraction of the hydrophilic black carbon acts as a contact ice nucleus at temperatures between 0° and −35°C, then increases in aerosol concentration from preindustrial times to the present day pose a new indirect effect, a glaciation indirect effect, on clouds. Here increases in contact ice nuclei in the present-day climate result in more frequent glaciation of supercooled clouds and increase the amount of precipitation via the ice phase. This reduces the cloud cover and cloud optical depth of midlevel clouds in mid and high latitudes and results in more absorption of solar radiation within the earth–atmosphere system. Therefore, this effect can at least partly offset the cloud lifetime effect.

Evidence of submicron desert dust as an effective ice nucleus at temperatures warmer than required for homogeneous freezing was recently obtained from continuous flow diffusion chamber data when sampling Asian dust particles (DeMott et al. 2003). Mildly supercooled altocumulus clouds at temperatures between −5° to −9°C were already glaciated in an event where the air mass originated from the Sahara, suggesting that Saharan submicron dust particles are effective ice nuclei (Sassen et al. 2003).

Dust, however, can be composed of different chemical species. Clay or silicate particles, contained in mineral aerosols, are effective ice nuclei (Chen et al. 1998; Pruppacher and Klett 1997). Kaolinite and montmorillonite are frequently used as surrogates for atmospheric dust particles in laboratory experiments because they are considered to be the main components of ice-nucleating tropospheric mineral dusts in the submicrometer range (Kumai 1961; Kumai and Francis 1962; Zuberi et al. 2002). Illite is another mineral dust that dominates the submicron clay fraction at certain locations (Claquin et al. 1999; Usher et al. 2003). Because the immersion freezing behavior of illite is very similar to that of montmorillonite (Diehl and Wurzler 2004), if no contact freezing experiments of illite are available, we use montmorillonite as a surrogate for both minerals. Quartz minerals, on the other hand, may dominate the mass of certain mineral dust aerosols (Schütz and Sebert 1987; Claquin et al. 1999), but do not act as efficient ice nuclei (Mason and Maybank 1958). Second, because they are predominantly contained in the coarse mode fraction (Schütz and Sebert 1987), they hardly reach the midtroposphere, additionally limiting their importance as ice nuclei. One problem in using natural soils for freezing experiments is that they may be contaminated with bacteria, which can be very efficient ice nuclei (Schnell and Vali 1976; Yankofsky et al. 1981; Diehl et al. 2002). Thus, in order to investigate pure mineral dust particles of known freezing behavior, we limit ourselves to the freezing of kaolinite as an example of a less efficient ice nucleus and montmorillonite as a surrogate for a more efficient ice nucleus.

In this paper, a new parameterization of immersion freezing for mixed-phase clouds between 0° and −35°C as described in the next section is employed. Dust is assumed to be composed either entirely of kaolinite or montmorillonite because these were the only two mineral dust components for which a temperature dependence for both contact and immersion freezing could be derived. The effectiveness of contact and immersion freezing of kaolinite, montmorillonite, and black carbon as a function of temperature is parameterized from a compilation of laboratory data by Diehl and Wurzler

(2004) and Diehl et al. (2005). In section 3, we establish the feasibility of the new parameterization and the temperature-dependent freezing properties of dust and black carbon in the present-day climate by comparing the climate model results to different observations. Thereafter, the impact of immersion and contract freezing of black carbon and dust for the anthropogenic indirect aerosol effect is evaluated in section 4 followed by discussion and conclusions in section 5.

2. Model description

We use the ECHAM4 general circulation model (GCM; Roeckner et al. 1996) to estimate the importance of immersion and contact nucleation of black carbon and dust aerosols on a global scale. The version of ECHAM4 used in this study includes a fully coupled aerosol–cloud microphysics module as described by Lohmann et al. (1999) and Lohmann (2002b, 2004). Here, prognostic equations for the mass-mixing ratio of dimethyl sulfide, sulfur dioxide, sulfate aerosols, methane sulfonic acid, hydrophobic and hydrophilic organic and black carbon aerosols; accumulation and coarse mode dust and sea salt aerosols; as well as for the mass mixing ratios of cloud liquid water and ice and number concentrations of cloud droplets and ice crystals are solved. Transport, dry and wet deposition, and chemical transformations of the aerosols and gaseous precursors are calculated on line with the GCM (Feichter et al. 1996). The aerosol number concentration is obtained by assuming an externally mixed aerosol (Lohmann 2002b).

The cloud microphysical parameterizations, except for the heterogeneous freezing in mixed-phase clouds described below, are identical to the model setup used in Lohmann (2004) assuming that snow crystals can be approximated as planar crystals for the riming rate between snow crystals and cloud droplets. The results from this simulation in which the ice nuclei concentration is independent of the chemical composition of the nuclei (referred to as simulation CTL) are included for reference below. We account for autoconversion of cloud droplets, accretion of cloud droplets by rain and snow, evaporation of cloud droplets and rain, aggregation of ice crystals, self-collection of ice crystals, accretion of ice crystals by snow, homogeneous and heterogeneous freezing of cloud droplets, secondary production of ice crystals (the Hallet–Mossop process), and melting and sublimation of ice crystals and snow (Lohmann 2002b). Cirrus cloud formation is limited to homogeneous freezing of supercooled aerosol particles (Lohmann and Kärcher 2002) because there is currently no parameterization that can capture the competition between homogeneous and heterogeneous nucleation in cirrus clouds (Kärcher and Lohmann 2003).

Between 0° and −35°C, the ice phase can be initiated by immersion freezing or contact nucleation in the model. Contact nucleation depends on the contact nuclei concentration and aerosol diffusivity following Levkov et al. (1992). It is parameterized as (m^{-3} s^{-1})

$$Q_{\mathrm{frz,cnt}} = m_{\mathrm{io}} D_{\mathrm{ap}} 4\pi r_l N_{a,\mathrm{cnt}} \frac{N_l^2}{\rho q_l}, \tag{1}$$

where r_l is the volume mean droplet radius, q_l is the cloud liquid water mass-mixing ratio in the cloudy part of the grid box, N_l is the number concentration of cloud droplets, ρ is the air density, T is the temperature, $m_{\mathrm{io}} = 10^{-12}$ kg is the original mass of a newly formed ice crystal, and D_{ap} is the Brownian aerosol diffusivity. It is given by

$$D_{\mathrm{ap}} = \frac{kTC_c}{6\pi\eta r_m}, \tag{2}$$

where k is the Boltzmann constant, T is the temperature, η is the viscosity of air $\{\eta = 10^{-5}\,[1.718 + 0.0049\,(T - T_o) - 1.2 \cdot 10^{-5}\,(T - T_o)^2]$ in kg m^{-1} $s^{-1}\}$, r_m is the aerosol mode radius, and C_c is the Cunningham correction factor $[C_c = 1 + 1.26(\lambda/r_m)(p_o/p)(T/T_o)]$. The aerosol mode radius is taken to be 0.39 μm for dust in the accumulation mode and 0.012 μm for black carbon (Hess et al. 1998); λ is the molecular free pathlength of air ($\lambda = 0.066$ μm), and p_o and T_o refer to standard condition of 101 325 Pa and 273 K.

Here, $N_{a,\mathrm{cnt}}$ is the number of contact nuclei. In simulation CTL, $N_{a,\mathrm{cnt}}$ is given as $N_{a,\mathrm{cnt}} = N_{\mathrm{ao}}\,(270.15 - T)^{1.3}$ following Young (1974) where $N_{\mathrm{ao}} = 2 \times 10^5$ m^{-3} is the number of active ice nuclei after Cotton et al. (1986). This is not realistic because the aerosol species that act as ice nuclei, such as mineral dust, soot, and biological material exhibit regional differences. Therefore the number of contact and immersion nuclei is related to mineral dust and black carbon in the sensitivity simulations carried out in this study as discussed below. Dust aerosols are limited to accumulation mode particles, because their mode radius of 0.39 μm closely matches the radius of 0.375 μm, for which Hung et al. (2003) found the dominant contribution to the overall ice mass. Moreover, the larger particles will hardly reach the midtroposphere. We chose to consider only the hydrophilic black carbon because laboratory studies by Gorbunov et al. (2001) suggested that the ability of black carbon to act as an ice nucleus increases with the number of OH groups on its surface. Also, in order for black carbon to be submerged in a cloud droplet prior to initiating immersion freezing, it needs to be hydrophilic.

A new parameterization of immersion freezing fol-

lowing Diehl and Wurzler (2004) is included in ECHAM4. It is given by

$$Q_{\text{frz,imm}} = N_{a,\text{imm}} \exp(273.2 - T) \frac{dT}{dt} \frac{\rho q_l}{\rho_l}, \qquad (3)$$

where ρ_l is the water density, and $N_{a,\text{imm}}$ is the number of immersion nuclei. This parameterization was compared to the Bigg equation (Bigg 1953), which is often used in models to describe immersion freezing. Drop freezing according to Bigg (1953) matches the results obtained for montmorillonite particles well but it significantly overestimates freezing by kaolinite and soot particles (Diehl and Wurzler 2004). Inherent in both the immersion and contract freezing parameterizations is the assumption that freezing is independent of aerosol size, because the laboratory studies, in which freezing was investigated in terms of the median freezing temperature, were not conducted in a way that any particle size dependence could be inferred (Mason and Maybank 1958; Pitter and Pruppacher 1973). A size dependence was, however, found in the studies by Gorbunov et al. (2001) and Hung et al. (2003). Here, we take the size dependence of black carbon as a contact nucleus into account by conducting sensitivity simulations with different freezing efficiencies that represent different aerosol sizes. The size dependence of dust is realized by restricting the dust ice nuclei to accumulation size as explained above.

In the model, the number of the contact ($N_{a,\text{cnt}}$) and immersion ice nuclei ($N_{a,\text{imm}}$) that enters Eqs. (1) and (3) is obtained from the fraction of aerosol particles made up by hydrophilic black carbon and accumulation mode dust aerosols, respectively, multiplied by a temperature dependence of the individual species. This temperature dependence is obtained from the onset and median freezing temperature of the individual species as shown in Fig. 1 based on a compilation of laboratory data by Diehl and Wurzler (2004) and Diehl et al. (2005). This approach differs from the scenarios described in Lohmann (2002a), who assumed that only a certain arbitrary fraction of the hydrophilic black carbon acted as contact nuclei independent of temperature and who neglected any chemical species dependence in the immersion freezing process. Here we can consider all hydrophilic black carbon aerosols as potential freezing nuclei, because the limitation of black carbon to initiate freezing is now incorporated in the parameterizations described above. Also, Lohmann (2002a) did not explicitly consider the temperature dependency of dust as contact nuclei but used a generic increase in contact nuclei with decreasing temperature (Young 1974).

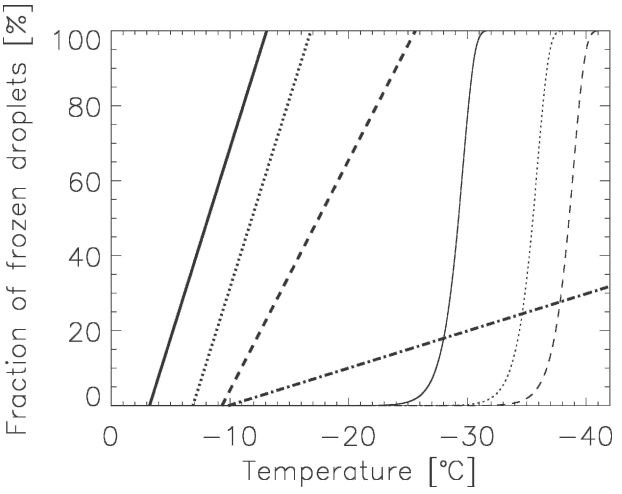

FIG. 1. Percentage fraction of cloud droplets frozen as a function of ice nuclei composition. Thick lines refer to contact freezing of montmorillonite (solid line), kaolinite (dotted line), and black carbon with radii of 1 μm (dashed lines), and to black carbon aerosols with radii of 0.3 μm (dot–dashed line). Thin lines refer to immersion freezing of the same aerosol particles. The immersion freezing results are valid for a 10-μm cloud droplet.

As shown in Fig. 1, contact freezing is always initiated at higher temperatures than immersion freezing. It is, however, limited by the collision efficiency. Montmorillonite is active as an ice nucleus at the highest temperature, followed by kaolinite and then black carbon for both freezing mechanisms. The size dependence of black carbon is realized by assuming freezing of two different sizes, the dashed line assumes maximum freezing efficiencies, which, strictly speaking, corresponds to black carbon particles of 1-μm radius. This size is comparable to the size of the dust particles used by Pitter and Pruppacher (1973), and much smaller than the pollen and leaf litter of up to 35-μm radius investigated by Diehl and Wurzler (2004) and Diehl et al. (2005). Thus, the shape of the freezing curve for the large soot particles fits better to the data for all other substances and was therefore included in the reference simulations KAO and MON. We added sensitivity studies in which this maximum contact freezing efficiency of black carbon was replaced by its mean freezing efficiency (Fig. 1, dot–dashed line). This mean contact freezing efficiency of black carbon corresponds to black carbon particles of 0.3-μm radius. It is lower than all the other freezing efficiencies and in disagreement with the general result from laboratory studies that contact nucleation is more efficient than immersion freezing (Diehl and Wurzler 2004; Diehl et al. 2005).

In the subsequent climate model simulations, we assume dust to be either composed of kaolinite or montmorillonite with different contact nucleation efficien-

TABLE 1. Sensitivity simulations.

Simulation	Description
KAO	Assuming dust to be composed of kaolinite
MON	Assuming dust to be composed of montmorillonite
KAO-meanBC	As KAO, but using the mean contact freezing efficiencies for black carbon
MON-meanBC	As MON, but using the mean contact freezing efficiencies for black carbon
CTL	Reference simulation, in which both contact and immersion freezing are independent of the chemical composition of the ice nuclei

cies of black carbon (see Table 1). Each simulation consists of a 10-yr run in T30 horizontal resolution (3.75° × 3.75°) and 19 vertical layers with the top at 10 hPa using climatological sea surface temperature after an initial spinup of three months. The following emissions and assumptions are used: present-day emissions of sea salt and dust as described in Lohmann (2002b); emissions of organic and black carbon, dimethylsulfide and sulfur dioxide as described in Lohmann et al. (2000); 80% of the black carbon emission are hydrophobic (Cooke et al. 1999), and is converted into hydrophilic black carbon by assuming an exponential aging time of 24 h (Lohmann 2002b).

3. Model evaluation

a. Annual latitude–pressure cross sections

To better understand the differences between simulations MON and KAO, the contribution of the individual freezing mechanisms to the total freezing rate are shown in Figs. 2 and 3. As expected from Fig. 1 most of the heterogeneous freezing in supercooled clouds between 0° and −35°C is initiated by contact freezing of

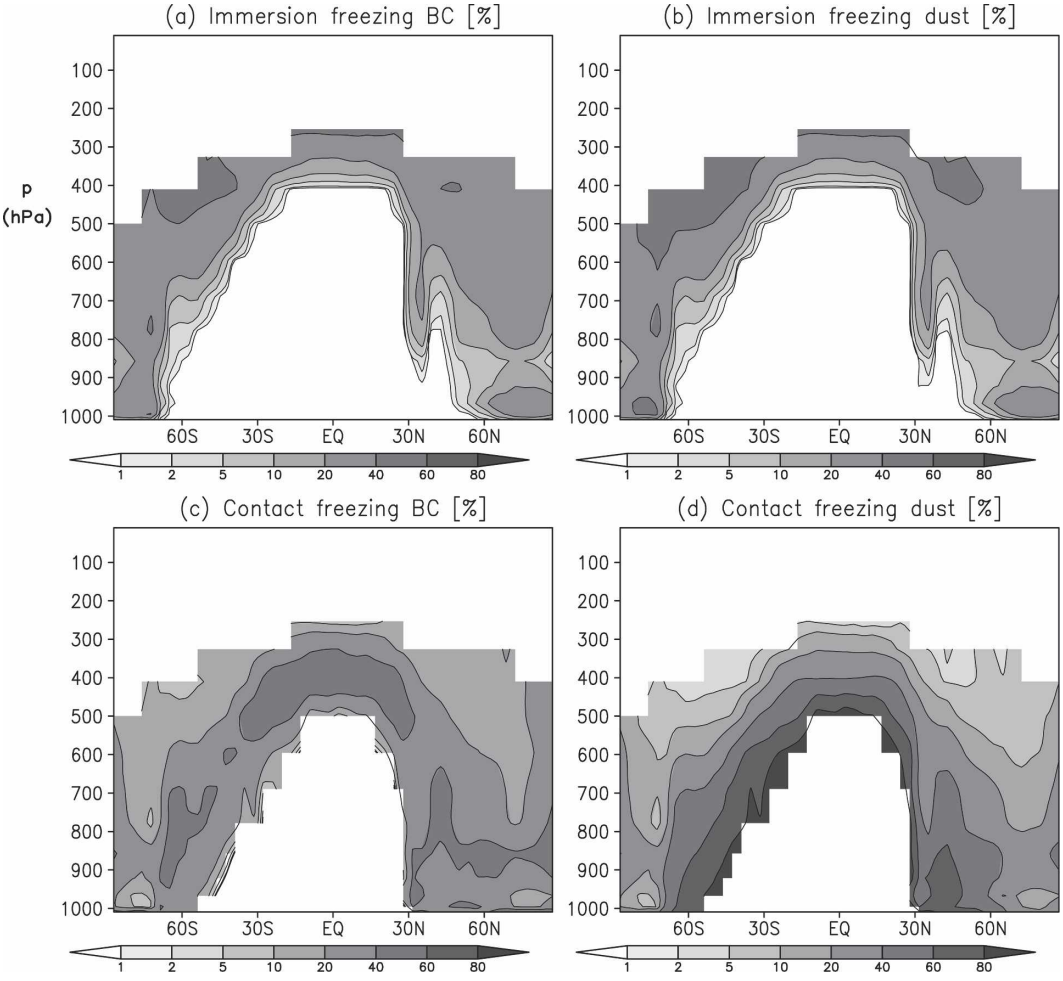

FIG. 2. Ten-year average of the annual zonal mean latitude vs pressure cross sections of the percentage fraction of the different freezing mechanisms from simulation KAO: (a) immersion freezing of black carbon, (b) immersion freezing of dust, (c) contact freezing of black carbon, and (d) contact freezing of dust.

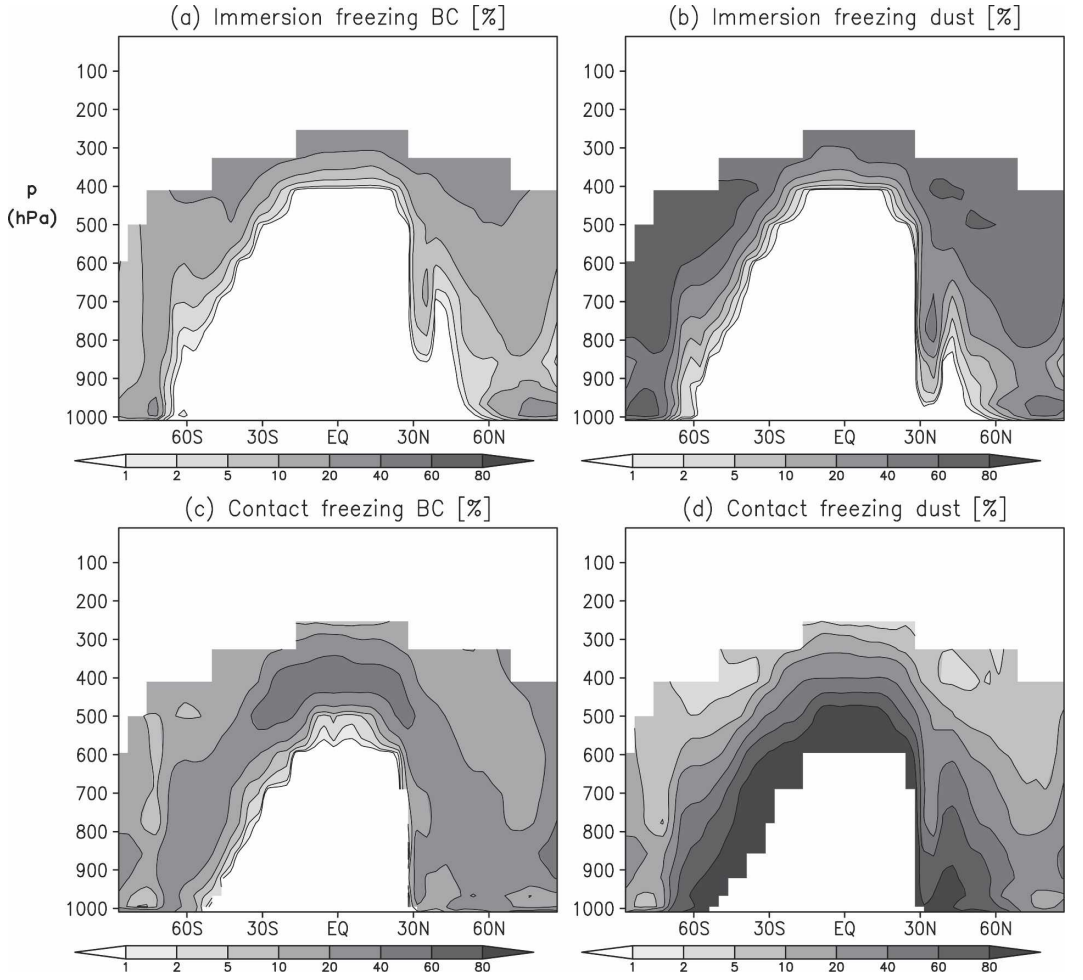

FIG. 3. As in Fig. 2 but for the simulation MON.

dust in both simulations especially at higher temperatures. If dust is assumed to be composed of montmorillonite as in simulation MON, immersion freezing of dust is the second most important freezing mechanism. In this simulation, immersion freezing of black carbon only exceeds 20% at the coldest temperatures because dust aerosols are far less abundant than black carbon aerosols (Fig. 4). In simulation KAO, freezing of black carbon is more important because freezing of kaolinite is less efficient than of montmorillonite (Fig. 1). Here, contact and immersion freezing of black carbon is as important as immersion freezing of dust, accounting for up to 40% of the freezing in different areas. Immersion freezing is most important at the coldest temperatures.

The number concentration of aerosol particles in Fig. 4 refers to the potential number of ice nuclei, before collision and before any temperature dependence of the freezing process is applied. Thus, a direct comparison with atmospheric measurements of ice nuclei, as carried out by Deshler and Vali (1992), for instance, is not possible because they inferred their concentration from the number of frozen droplets. Instead, we also show the ice crystal number concentration in Fig. 4. It is lower than the potential ice nuclei concentration. The maximum values of 1 cm^{-3} are in agreement with different in situ observations as described in Kärcher and Lohmann (2002).

b. *Annual zonal means*

The annual zonal mean vertical integral of the cloud liquid water content (liquid water path; LWP) over the oceans for the simulations KAO and MON is compared to satellite estimates of liquid water path from the Special Sensor Microwave Imager (SSM/I) by Greenwald et al. (1993) and Wentz (1997) is shown in Fig. 5. The simulated liquid water path is slightly larger in simulation KAO than in simulation MON because both the contact and the immersion freezing are less efficient for kaolinite than for montmorillonite (cf. Fig. 1). In the global annual mean, LWP over the oceans amounts to

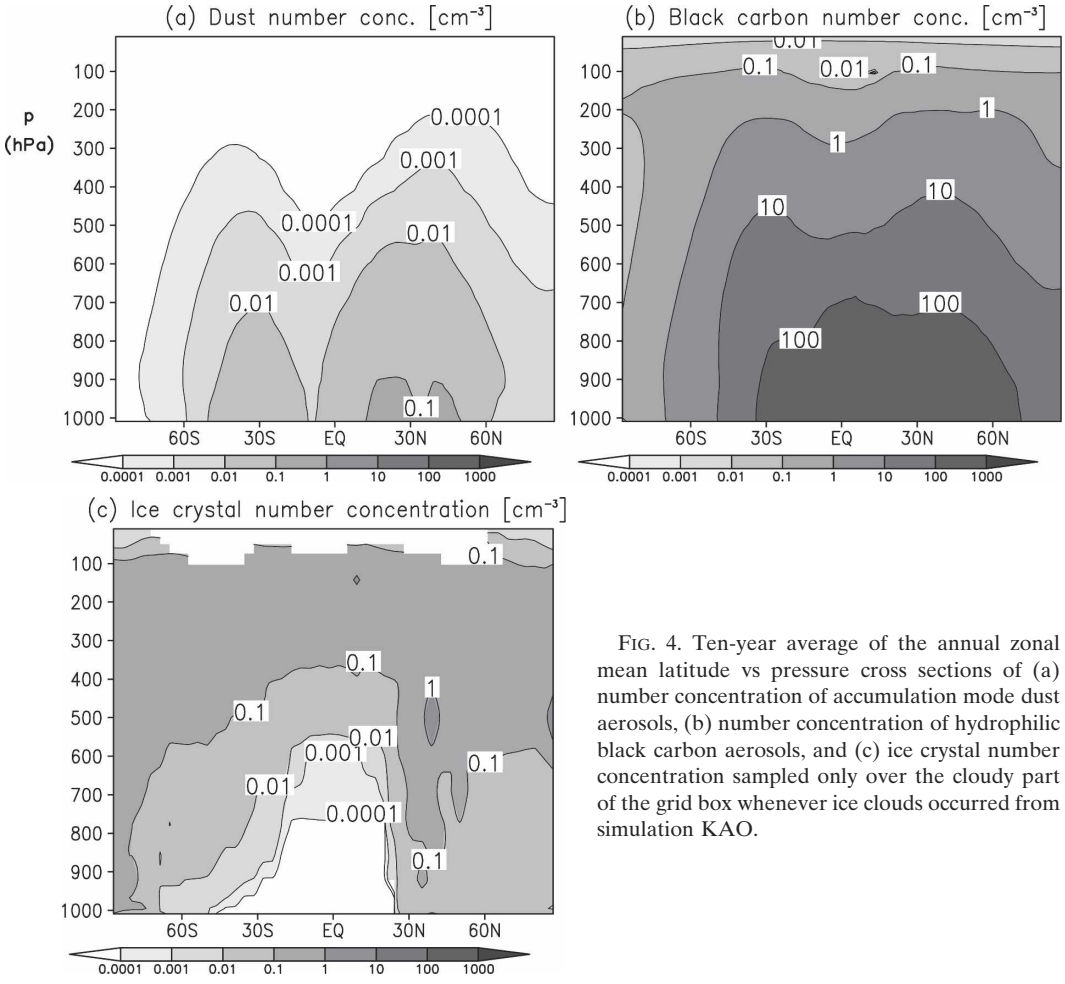

FIG. 4. Ten-year average of the annual zonal mean latitude vs pressure cross sections of (a) number concentration of accumulation mode dust aerosols, (b) number concentration of hydrophilic black carbon aerosols, and (c) ice crystal number concentration sampled only over the cloudy part of the grid box whenever ice clouds occurred from simulation KAO.

81.9 g m^{-2} in simulation KAO and 80.6 g m^{-2} in simulation MON. Both global mean values are in excellent agreement with the observations that amount to 79.5 g m^{-2} (Greenwald et al. 1993) and 83.7 g m^{-2} (Wentz 1997). Conversely, in the standard simulation CTL, in which ice nuclei are independent of the chemical composition, the global annual mean LWP over the oceans only amounts to 61.8 g m^{-2}. The zonal mean distribution is well captured in simulations MON and KAO with LWP peaks in the Tropics and the extratropical storm tracks.

The increase in liquid water path in simulations KAO and MON as compared to CTL suggests that ice crystal formation is limited by the availability of black carbon and dust. This reduces the precipitation efficiency especially in the Tropics (Fig. 5b), which is in better agreement with the observed precipitation data that are obtained from a variety of sources in the Global Precipitation Climatology Center (Stendel and Arpe 1997). In the global mean, simulation MON's precipitation rate of 2.65 mm day^{-1} agrees best with the observed precipitation of 2.74 mm day^{-1}, whereas in CTL the overestimation in the Tropics causes also the global-mean precipitation of 2.94 mm day^{-1} to be too high.

The shortwave cloud forcing, which is defined as the difference in the top-of-the-atmosphere (TOA) shortwave radiation between all-sky and clear-sky conditions is obtained from the Earth Radiation Budget Experiment (ERBE). It is most negative in areas with the highest liquid and ice water paths in the Tropics and in midlatitude storm tracks (Fig. 5c). In simulations MON and KAO, the maximum shortwave cloud forcing in the Southern Ocean is captured very well, while the corresponding peak on the Northern Hemisphere is underestimated. The maximum in the Tropics is too negative suggesting that the clouds are either too reflective or too abundant. A lower cloud abundance as in simulation CTL hence results in a lower shortwave cloud forcing in the Tropics. However, in this simulation, the shortwave cloud forcing is underestimated everywhere.

The interpretation of clouds being too reflective in simulations MON and KAO is in agreement with the

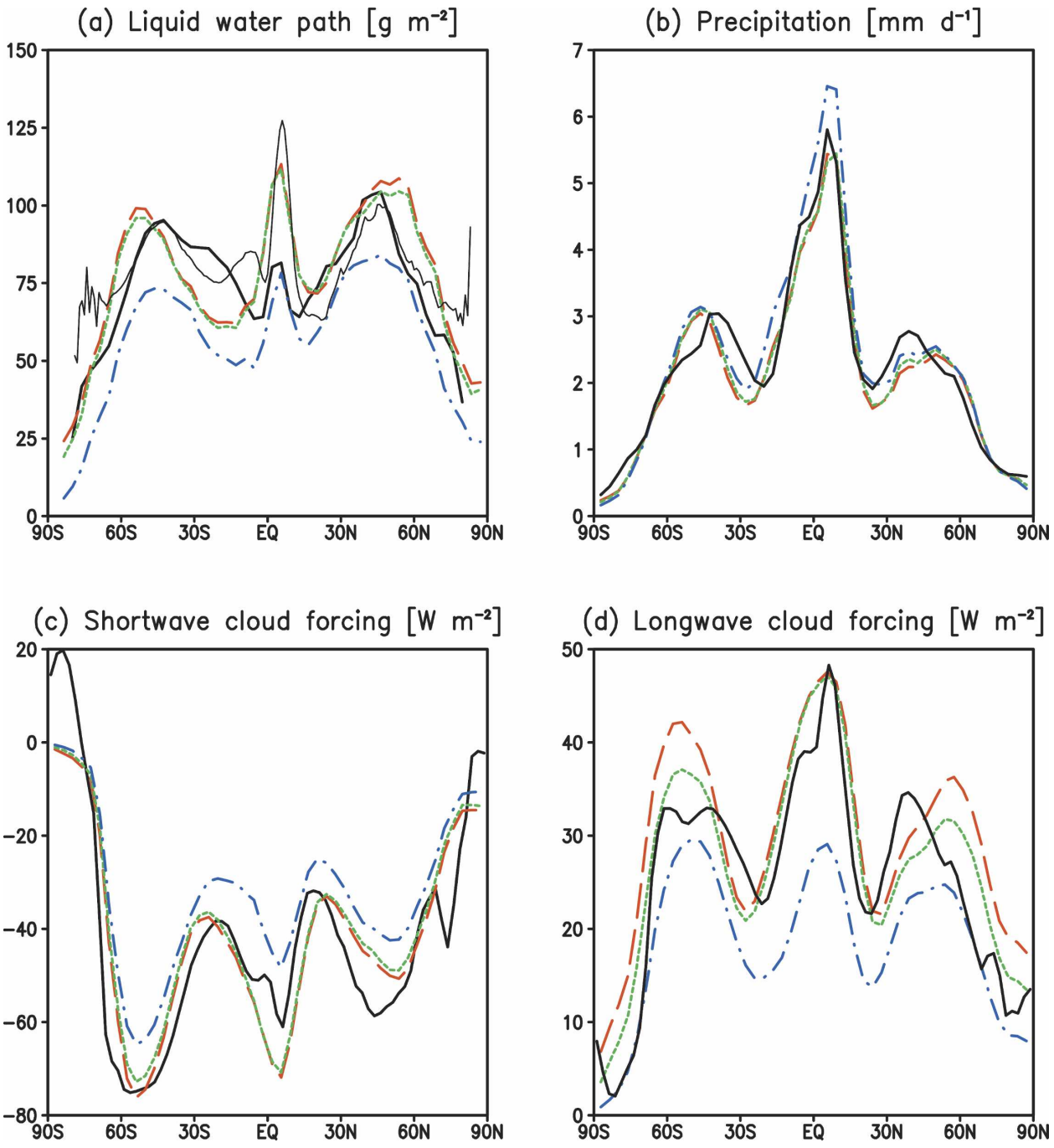

FIG. 5. Zonal, annual means of (a) LWP, (b) precipitation, (c) TOA SW, and (d) LW cloud forcing from the simulations KAO (red dashed lines), MON (green dotted lines), and CTL (blue dot–dashed lines) as compared with different observations (black solid lines). We include SSM/I retrievals of LWP from Greenwald et al. (1993; thick line) and Wentz (1997; thin line), precipitation data from the Global Precipitation Climatology Center (GPCC; Stendel and Arpe 1997) and shortwave and longwave cloud forcing from the ERBE.

comparison of longwave cloud forcing (Fig. 5d). In contrast to the shortwave cloud forcing, longwave cloud forcing mainly depends on the cloud water and ice mass mixing ratio and the cloud height, that is, temperature, but depends only weakly on the cloud droplet and ice crystal size. Its good agreement in the Tropics with observations in simulations MON and KAO thus indicates that the cloud droplets are too small, hence too highly reflective. Discrepancies between simulations MON and KAO are most prevalent in the midlatitudes. Here

the longwave cloud forcing is larger in simulation KAO because ice crystals are nucleated at colder temperatures, that is, higher altitudes, thus reducing the outgoing longwave radiation more effectively.

Overall, simulation MON is in best agreement with these different zonal annual mean observations. This indirectly validates the new parameterization suggesting that the properties of ice nuclei in the climate model should follow the mixture of hydrophilic black carbon and dust assumed to be composed of montmorillonite.

c. Comparison with field data

One caveat when trying to validate climate model output with data from field experiments is that a climate model cannot be expected to capture individual events. However, if statistical relationships are derived from these field data, they can be compared to climate model data because statistical correlations are temporally and spatially more robust than individual measurements. Here, we compare the size and number concentration of cloud droplets and ice crystals as a function of temperature between 0° and −35°C with stratiform cloud observations taken from different field projects over Canada in winter, spring, and fall (Korolev et al. 2003). We took model data from the same months (December–April, September–October) and the same region as the observations were taken. In the model the same ice crystal density of 800 kg m^{-3} that Korolev et al. (2003) applied to their data is used for computing the mean volume radius of ice crystals.

In the observations, the distinction between ice and liquid is based on the ratio of the ice water content (IWC) to the total water content (TWC) from separate measurements of the liquid and total water content with different sensors of the Nevzorov probe (Korolev et al. 1998). Clouds are considered liquid when the ratio IWC/TWC is less than 10% and ice, when the ratio IWC/TWC exceeds 90% (Korolev et al. 2003). Two different Forward Scattering Spectrometer Probes (FSSP-100) were used for inferring ice particle concentrations of particles smaller than 32 and 95 μm, respectively, in glaciated clouds. This information when combined with an ice water content measurement from the Nevzorov probe can be used to obtain an estimate of ice crystal size. The FSSP inlet may cause shattering of ice crystals during sampling that could result in an overestimation of the ice crystal number concentration up to a factor of 2 to 3 (Field et al. 2003). This translates into an error in ice particle size of 25%–45% as indicated in Figs. 6 and 7. These ice particle size estimates are, however, in good agreement with measurements of particle size using a different technique (Korolev et al. 2001). The error in the cloud droplet number concentration from the FSSP is estimated to be ≤15% and that in the ice crystal number concentration from the 2D-C data ≤20% (A. Korolev 2005, personal communication).

As shown in Fig. 6, the ice crystal number concentration is rather constant with temperature in the observations with values between 1 and 10 cm^{-3} as deduced from the FSSP data (Korolev et al. 2003), and concentrations between 3 and 6 L^{-1} for particles >125 μm obtained from the optical 2D-C probe (Gultepe et al. 2001). The simulated ice crystal concentrations fall in between the concentrations deduced from the FSSP data and the 2D-C probe. This tendency was also observed when the Canadian climate model was compared to ice crystal concentrations obtained from the FSSP and 2D-C probe in the Arctic (Lohmann et al. 2001). In simulation CTL, the ice crystal number concentration steadily increases with decreasing temperature. It mirrors the increase in ice nuclei concentration with decreasing temperature (Young 1974). However, this temperature dependence is not reflected in the observed ice crystal number concentration probably due to different ice multiplication processes and the decrease in ice nuclei concentration with decreasing altitude, that is, colder temperatures. In the model, only the Hallett–Mossop process is parameterized, which is responsible for ice multiplication between −3° and −8°C. If the freezing process is associated with different chemical species that are less abundant at colder temperatures as in simulations KAO and MON, the ice crystal number concentration is rather constant between −5° and −25°C in better agreement with observations.

The cloud droplet size decreases with decreasing temperature in the model (Fig. 7) as one would expect from the smaller amount of water vapor present at colder temperatures in case of a temperature independent cloud droplet number concentration. This, however, agrees with the observations only at temperatures above −10°C because the cloud droplet number decreases at temperatures below −7.5°C in the observations while it is rather constant in the model (Fig. 6). The increase in cloud droplet size with decreasing temperatures below −20° in the observations is believed to be an artifact. It could either stem from an increasing contamination with ice crystals at these colder temperatures (G. Isaac 2004, personal communication), or could be caused by the limited dataset at the coldest temperatures (Gultepe et al. 2001).

The observed ice crystal size is largest between −10° and −15°C, which is consistent with the maximum diffusional growth range of ice (Korolev et al. 2003). In simulations MON and KAO, the ice crystals are larger

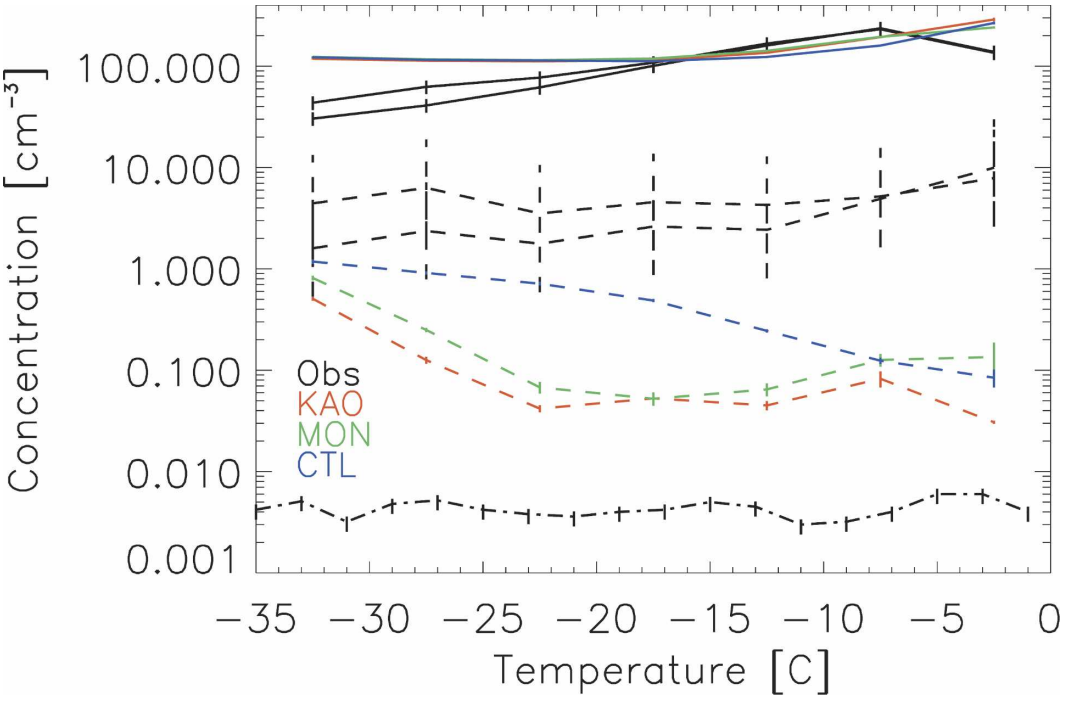

FIG. 6. Cloud droplet (solid lines) and ice crystal (dashed lines) number concentrations as a function of temperature deduced from two different FSSP probes in field experiments over Canada (Korolev et al. 2003), and the three model simulations together with their standard errors. Vertical bars in the observations refer to the estimated error in the number concentrations. Ice crystal number concentrations from the 2D-C probe for particles >125 μm (dashed–dotted line) from the same Canadian datasets (Gultepe et al. 2001) are included as well.

than observed at temperatures below −10°C and the maximum sizes occur between −25° and −20°C rather than at the temperature of maximum diffusional growth (Fig. 7). The problem could be caused by the data used for validation as the FSSP probes detects 3 orders of magnitude more crystals than the 2D-C probe (Fig. 6). In summary, both simulations KAO and MON agree reasonably well with the different observations and are rather similar to each other. Thus, both of them will be used in the subsequent climate change simulations.

4. Implications of the nature of dust nuclei for the indirect aerosol effect

Robust climate change estimates are not possible at this point, because of the uncertainties related to dust composition, the neglect of dust effects on cirrus clouds, the insufficient knowledge of ice multiplication processes and the uncertainty related to the scarcity of heterogeneous freezing data for mixed-phase clouds. Therefore the results described below are only sensitivity studies, discussing a few of the many possible scenarios.

The question here is whether the total anthropogenic indirect aerosol effect on the net radiation at TOA, that is, the total of all aerosol effects on warm, mixed-phase and ice clouds (from here on just termed indirect aerosol effect), depends on the nature of the dust aerosols and their effectiveness as freezing nuclei. To estimate the indirect aerosol effect, all 10-yr simulations were rerun, but without any anthropogenic emissions. That is, emissions of sulfur dioxide and carbonaceous aerosols from fossil fuel and biomass burning are set to zero. It leaves natural emissions from forests as the only source for organic carbon, and dimethyl sulfide emissions from the ocean and volcanoes as the only sources for sulfate aerosols. Greenhouse gas concentrations and sea surface temperatures are held constant at their present-day value.

The change in aerosol optical depth basically represents the forcing for these simulations. As shown in Fig. 8 it is largest in the midlatitudes of the Northern Hemisphere. Because an increase in the aerosol number concentration increases the number of cloud droplets, the autoconversion rate, which depends inversely on the number of cloud droplets, is reduced in the present-day simulations as compared to the preindustrial climate. Hence, the liquid water path is increased in all simulations, most noticeably in the Northern Hemisphere. The magnitude of the increase in liquid water path in

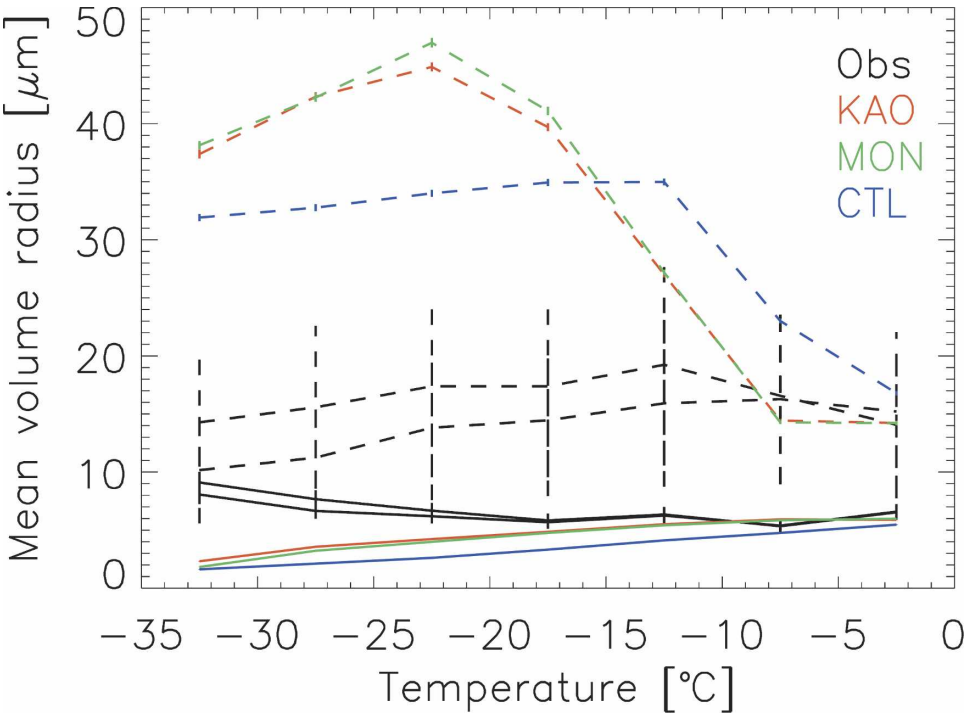

FIG. 7. Average mean volume radii for cloud droplets (solid lines) and ice crystals (dashed lines) as a function of temperature from different observations over Canada (Korolev et al. 2003), and the three model simulations together with their standard errors. The observational data and their errors stem from the Nevzorov total water probes combined with two different FSSP probes.

the Northern Hemisphere depends on the nature of the dust particles. If dust is assumed to be composed of kaolinite, whose freezing is not as effective as that of montmorillonite, then the addition of black carbon has a larger influence (cf. Fig. 2). Thus, the liquid water path even decreases at high latitudes and the increase in ice water path is larger in simulation KAO than in simulation MON (Fig. 8; Table 2). The larger increase in liquid water path in simulation MON results in a decrease in precipitation as is expected from the indirect cloud lifetime effect. Similar results to simulation MON are obtained from simulation CTL, where the freezing of cloud droplets is independent of the chemical nature of the ice nuclei.

If, on the other hand, the freezing of black carbon is more effective as in simulation KAO, the supercooled cloud is glaciated more rapidly. Because the precipitation formation via the ice phase is more efficient than in warm clouds, these glaciated clouds have a shorter lifetime than supercooled water clouds (Rogers and Yau 1989). Thus the global mean cloud cover decreases from preindustrial to the present day in simulation KAO but slightly increases in simulations MON and CTL (Fig. 8; Table 2).

A similar opposing behavior was found in Lohmann (2002a) when the fraction of hydrophilic black carbon that served as contact ice nuclei was increased from 0% to 10%. Those simulations represented more extreme situations in which the global mean increase in liquid water path in the simulation without black carbon as contact ice nuclei turned into a decrease once 10% of the hydrophilic black carbon acted as contact ice nuclei. The results from simulations KAO and MON suggest even the subtle change of the nature of dust aerosols is sufficient in determining the sign of the change in cloud cover and precipitation in response to anthropogenic aerosol particles (Table 2). This fragility of the hydrological cycle to the concentration of ice nuclei has been observed on a cloud scale for quite some time from weather modification studies (see, e.g., Bruintjes 1999). However, the confidence is low at scales beyond the cloud scale.

The decrease in net radiation at TOA due to anthropogenic aerosol particles amounts to 2–2.1 W m^{-2} in simulations KAO and KAO-meanBC but only to 1 W m^{-2} in simulations MON, MON-meanBC, and CTL, (Table 2). In simulations KAO and KAO-meanBC, the increase in liquid water path that leads to a larger reflection of shortwave radiation at TOA competes with the decrease in cloud cover that leads to more absorp-

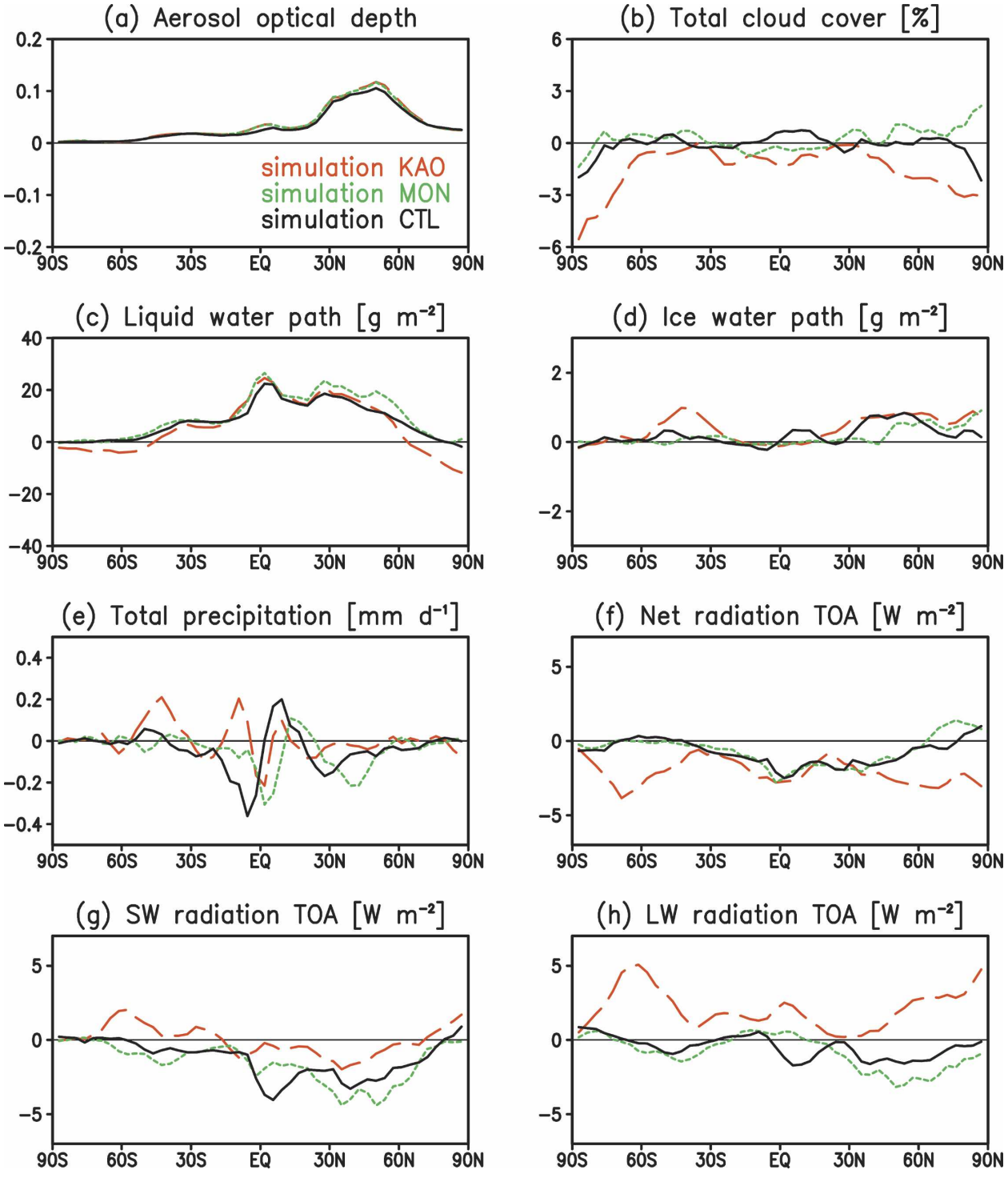

FIG. 8. Zonal, annual mean changes in (a) aerosol optical depth, (b) total cloud cover, (c) LWP (g m^{-2}), (d) ice water path (g m^{-2}), (e) total precipitation (mm day^{-1}), (f) TOA net, (g) SW-, and (h) LW-radiation between preindustrial and present-day times for the reference simulation CTL (black solid line), simulation KAO (red dashed line), and MON (green dotted line).

TABLE 2. Global annual mean changes ± interannual std devs of aerosol optical depth ($\Delta\tau$), LWP (ΔLWP), ice water path (ΔIWP), total cloud cover (ΔTCC), precipitation (ΔPR), SW (ΔF_{SW}), LW (ΔF_{LW}), and net radiation (ΔF_{net}) at the top of the atmosphere between the different preindustrial and different present-day simulations.

Simulation	CTL	KAO	MON	KAO-meanBC	MON-meanBC
$\Delta\tau$	0.04 ± 0.001	0.04 ± 0.001	0.04 ± 0.001	0.04 ± 0.001	0.04 ± 0.001
ΔLWP (g m^{-2})	10.5 ± 0.69	9.83 ± 0.61	12.73 ± 0.39	12.38 ± 0.29	14.42 ± 0.40
ΔIWP (g m^{-2})	0.20 ± 0.09	0.35 ± 0.04	0.10 ± 0.03	0.17 ± 0.04	−0.01 ± 0.03
ΔTCC (%)	0.07 ± 0.38	−1.00 ± 0.26	0.12 ± 0.16	−0.61 ± 0.21	0.40 ± 0.27
ΔPR (mm day^{-1}),	−0.051 ± 0.008	0.005 ± 0.007	−0.052 ± 0.008	−0.019 ± 0.005	−0.066 ± 0.006
ΔF_{SW} (W m^{-2})	−1.63 ± 0.39	−0.22 ± 0.24	−1.77 ± 0.14	−1.04 ± 0.16	−2.23 ± 0.12
ΔF_{LW}* (W m^{-2})	−0.59 ± 0.34	1.78 ± 0.22	−0.74 ± 0.15	1.03 ± 0.20	−1.18 ± 0.24
ΔF_{net} (W m^{-2})	−1.04 ± 0.27	−2.00 ± 0.20	−1.02 ± 0.19	−2.08 ± 0.12	−1.05 ± 0.19

* For easier understanding and in accordance with reports on observed changes in emitted longwave radiation (e.g., Wielicki et al. 2002), here a positive change in longwave radiation means that more longwave radiation is emitted to space. This differs from the earlier ECHAM4 GCM studies on indirect aerosol effects where the GCM notation of upward fluxes being negative fluxes was kept.

tion of solar radiation in the earth–atmosphere system, resulting in a rather small decrease in the TOA net shortwave radiation up to 1 W m^{-2}. The reduced cloud cover, on the other hand, results in more longwave radiation being emitted to space so that the decrease in TOA net radiation is larger than the decrease in TOA shortwave radiation in these experiments. In simulations CTL, MON, and MON-meanBC, the slight increase in cloud cover aggravates the increase in liquid water path thus reducing the TOA net shortwave radiation by 1.6 to 2.2 W m^{-2}. Part of that reduction in shortwave radiation is compensated by a reduced amount of longwave radiation emitted to space in response to the larger cloud cover in simulations CTL, MON, and MON-meanBC.

In summary, the indirect aerosol effect in simulation MON is comparable to simulation CTL in which heterogeneous freezing is independent of the chemical and physical nature of the ice nuclei. The switch from a reduction in precipitation due to the indirect aerosol cloud lifetime effect in simulation MON to a slight increase in precipitation due to the glaciation indirect aerosol effect in simulation KAO is caused by heterogeneous nucleation of black carbon. This effect is not seen in simulation MON because montmorillonite freezes so effectively that black carbon only plays a minor role as a heterogeneous ice nucleus.

5. Discussion and conclusions

A new parameterization of immersion freezing for black carbon and mineral dust assumed to be composed of either kaolinite (simulation KAO) or montmorillonite (simulation MON) is introduced into the ECHAM4 general circulation model. In addition, the effectiveness of black carbon and dust as ice nuclei as a function of temperature for both contact and immersion freezing is parameterized from a compilation of laboratory studies by Diehl and Wurzler (2004) and Diehl et al. (2005). This is the first time that freezing parameterizations take the chemical composition of ice nuclei into account. Montmorillonite serves as a contact ice nucleus at the highest temperatures followed by kaolinite and then by black carbon. Immersion freezing sets in at lower temperatures in the same succession for the different chemical species.

Comparison of the simulated present-day climate with different observations does not show a clear preference for dust as a freezing nucleus to be composed of kaolinite or montmorillonite because most differences are rather subtle. These subtle differences between simulations KAO and MON have, however, large implications for the anthropogenic indirect aerosol effect. Here the decrease in net radiation at the TOA varies from 1 ± 0.3 W m^{-2} to 2.1 ± 0.1 W m^{-2} depending on whether dust is assumed to be composed of kaolinite or montmorillonite. The difference in the background dust composition is important for the prominence of black carbon as ice nuclei. In the simulations where dust is assumed to be kaolinite, black carbon has a higher relevancy as ice nuclei, because kaolinite is not freezing as effectively as montmorillonite. In simulation KAO, the addition of black carbon results in a larger ice water path and a slightly higher precipitation rate in the present-day climate as compared to preindustrial conditions, and a reduced total cloud cover. In simulation MON, on the other hand, the increase in the ice water path is much smaller, and globally the change in precipitation is dominated by the reduction in warm-phase precipitation due to the indirect cloud lifetime effect.

In all simulations, the change in longwave radiation at the TOA is not negligible but varies between 1.8 and −1.2 W m^{-2} (Table 2). This contribution of the longwave radiation is significantly larger than that in previ-

ous studies of the indirect aerosol effect that only considered the warm indirect aerosol effect. There the longwave effect amounted only to 0.1 to 0.4 W m^{-2} (Lohmann and Lesins 2002; Menon et al. 2002). In simulation CTL, where already some aerosol effects on mixed-phase clouds are considered, such that the riming rate of snow crystals with cloud droplets depends on the cloud droplet size, the longwave effect is enhanced to -0.6 W m^{-2} (Table 2). The sensitivity simulations carried out in this paper thus reinforce the point that aerosol effects on ice clouds are more complex than aerosol effects on warm clouds and that feedbacks within the climate system cannot be neglected. It also points to the necessity of discussing both the shortwave and the net radiative effects as evaluating only the aerosol indirect effect on the shortwave radiation can considerably over- or underestimate the indirect effect on the net radiation. For example, considering dust to be composed of montmorillonite as in simulations MON and MON-meanBC results in roughly twice the shortwave radiative effect as the net radiative effect, whereas in simulations KAO and KAO-meanBC, the decrease in shortwave radiation at the TOA amounts to at most half of the net radiative effect.

All these studies are sensitivity studies, discussing a few of the plausible scenarios. Uncertainties are related to the chemical composition of the dust aerosols as well as the ice formation mechanisms themselves. That is, if dust aerosols do not freeze like montmorillonite or kaolinite, the uncertainties could be either larger or smaller.

The big differences in the indirect aerosol effect in terms of the TOA radiation budget and the hydrological cycle that are caused by the nature of the background dust aerosols clearly require a better knowledge of the composition of dust aerosols in the atmosphere. This knowledge is also needed for the direct radiative effect of dust aerosols because dust aerosols can have a negative or positive radiative forcing depending on their mineralogical composition (Sokolik and Toon 1999). Thus, more measurements of the mineralogical composition of dust and its effectiveness as an ice nucleus are clearly needed.

Acknowledgments. Ulrike Lohmann is grateful for support from the National Science and Engineering Research Council of Canada (NSERC) and the Canadian Foundation for Climate and Atmospheric Sciences (CFCAS). She thanks the Deutsches Klimarechenzentrum for computing time and Alexei Korolev for providing the data from the Canadian research flights and useful discussions. We are grateful for comments and suggestions from Steve Ghan, Corinna Hoose, and three anonymous reviewers.

REFERENCES

Anderson, T. L., R. J. Charlson, S. E. Schwartz, R. Knutti, O. Boucher, H. Rodhe, and J. Heintzenberg, 2003: Climate forcing by aerosols—A hazy picture. *Science,* **300,** 1103–1104.

Bigg, E. K., 1953: The supercooling of water. *Proc. Phys. Soc.,* **66,** 688–694.

Bruintjes, R. T., 1999: A review of cloud seeding experiments to enhance precipitation and some new prospects. *Bull. Amer. Meteor. Soc.,* **80,** 805–820.

Chen, Y., S. M. Kreidenweis, L. M. McInnes, D. C. Rogers, and P. J. DeMott, 1998: Single particle analyses of ice nucleating aerosols in the upper troposphere and lower stratosphere. *Geophys. Res. Lett.,* **25,** 1391–1394.

Claquin, T., M. Schulz, and Y. J. Balkanski, 1999: Modeling the mineralogy of atmospheric dust sources. *J. Geophys. Res.,* **104,** 22 243–22 256.

Cooke, W. F., C. Liousse, H. Cachier, and J. Feichter, 1999: Construction of a 1 × 1 degree fossil fuel emission data set for carbonaceous aerosol and implementation and radiative impact in the ECHAM4 model. *J. Geophys. Res.,* **104,** 22 137–22 162.

Cotton, W. R., G. J. Tripoli, R. M. Rauber, and E. A. Mulvihill, 1986: Numerical simulation of the effects of varying ice crystal nucleation rates and aggregation processes on orographic snowfall. *J. Climate Appl. Meteor.,* **25,** 1658–1680.

DeMott, P. J., K. Sassen, M. R. Poellot, D. Baumgardner, D. C. Rogers, S. D. Brooks, A. J. Prenni, and S. M. Kreidenweis, 2003: African dust aerosols as atmospheric ice nuclei. *Geophys. Res. Lett.,* **30,** 1732, doi:10.1029/2003GL017410.

Deshler, T., and G. Vali, 1992: Atmospheric concentrations of submicron contact-freezing nuclei. *J. Atmos. Sci.,* **49,** 773–784.

Diehl, K., and S. Wurzler, 2004: Heterogeneous drop freezing in the immersion mode: Model calculations considering soluble and insoluble particles in the drops. *J. Atmos. Sci.,* **61,** 2063–2072.

——, C. Quick, S. Matthias-Maser, S. K. Mitra, and R. Jaenicke, 2001: The ice nucleating ability of pollen. Part I: Laboratory studies in deposition and condensation freezing modes. *Atmos. Res.,* **58,** 75–87.

——, S. Matthias-Maser, S. K. Mitra, and R. Jaenicke, 2002: The ice nucleating ability of pollen. Part II: Laboratory studies in immersion and contact freezing modes. *Atmos. Res.,* **61,** 125–133.

——, M. Simmel, and S. Wurzler, 2005: Numerical simulations on the impact of aerosol properties and freezing modes on the glaciation, microphysics, and dynamics of a convective cloud. *J. Geophys. Res.,* **110,** in press.

Feichter, J., E. Kjellström, H. Rodhe, F. Dentener, J. Lelieveld, and G.-J. Roelofs, 1996: Simulation of the tropospheric sulfur cycle in a global climate model. *Atmos. Environ.,* **30,** 1693–1707.

Field, P. R., R. Wood, P. R. A. Brown, P. H. Kaye, E. Hirst, R. Greenaway, and J. A. Smith, 2003: Ice particle interarrival times measured with a fast FSSP. *J. Atmos. Oceanic Technol.,* **20,** 249–261.

Gorbunov, B., A. Baklanov, N. Kakutkina, H. L. Windsor, and R. Toumi, 2001: Ice nucleation on soot particles. *J. Aerosol Sci.,* **32,** 199–215.

Greenwald, T. J., G. L. Stephens, T. H. Vonder Haar, and D. L. Jackson, 1993: A physical retrieval of cloud liquid water over the global oceans using Special Sensor Microwave/Imager (SSM/I) observations. *J. Geophys. Res.,* **98,** 18 471–18 488.

Gultepe, I., G. A. Isaac, and S. G. Cober, 2001: Ice crystal number concentration versus temperature for climate studies. *Int. J. Climatol.,* **21,** 1281–1302.

Hess, M., P. Koepke, and I. Schult, 1998: Optical properties of aerosols and clouds: The software package OPAC. *Bull. Amer. Meteor. Soc.,* **79,** 831–844.

Hung, H.-M., A. Malinowski, and S. T. Martin, 2003: Kinetics of heterogeneous ice nucleation on the surfaces of mineral dust cores inserted into aqueous ammonium sulfate particles. *J. Phys. Chem.,* **A107,** 1296–1306.

Jacobson, M. Z., 2001: Strong radiative heating due to the mixing state of black carbon in atmospheric aerosols. *Nature,* **409,** 695–697.

——, 2002: Control of fossil-fuel particulate black carbon and organic matter, possibly the most effective method of slowing global warming. *J. Geophys. Res.,* **107,** 4410, doi:10.1029/2001JD001376.

Kärcher, B., and U. Lohmann, 2002: A parameterization of cirrus cloud formation: Homogeneous freezing of supercooled aerosols. *J. Geophys. Res.,* **107,** 4010, doi:10.1029/2001JD000470.

——, and ——, 2003: A parameterization of cirrus cloud formation: Heterogeneous freezing. *J. Geophys. Res.,* **108,** 4402, doi:10.1029/2002JD003220.

Korolev, A. V., J. W. Strapp, G. A. Isaac, and A. N. Nevzorov, 1998: The Nevzorov airborne hot-wire LWC-TWC probe: Principle of operation and performance characteristics. *J. Atmos. Oceanic Technol.,* **15,** 1495–1510.

——, G. A. Isaac, I. P. Mazin, and H. W. Barker, 2001: Microphysical properties of continental clouds from in-situ measurements. *Quart. J. Roy. Meteor. Soc.,* **127,** 2117–2151.

——, ——, S. G. Cober, W. Strapp, and J. Hallett, 2003: Microphysical characterization of mixed-phase clouds. *Quart. J. Roy. Meteor. Soc.,* **129,** 39–65.

Kumai, M., 1961: Snow crystals and the identification of the nuclei in the northern United States of America. *J. Meteor.,* **18,** 139–150.

——, and K. E. Francis, 1962: Nuclei in snow and ice crystals on the Greenland ice cap under natural and artificially stimulated conditions. *J. Atmos. Sci.,* **19,** 474–481.

Levin, Z., and S. A. Yankofsky, 1983: Contact versus immersion freezing of freely suspended droplets by bacterial ice nuclei. *J. Climate Appl. Meteor.,* **22,** 1964–1966.

Levkov, L., B. Rockel, H. Kapitza, and E. Raschke, 1992: 3D mesoscale numerical studies of cirrus and stratus clouds by their time and space evolution. *Beitr. Phys. Atmos.,* **65,** 35–58.

Lohmann, U., 2002a: A glaciation indirect aerosol effect caused by soot aerosols. *Geophys. Res. Lett.,* **29,** 1052, doi:10.1029/2001GL014357.

——, 2002b: Possible aerosol effects on ice clouds via contact nucleation. *J. Atmos. Sci.,* **59,** 647–656.

——, 2004: Can anthropogenic aerosols decrease the snowfall rate? *J. Atmos. Sci.,* **61,** 2457–2468.

——, and J. Feichter, 2001: Can the direct and semi-direct aerosol effect compete with the indirect effect on a global scale? *Geophys. Res. Lett.,* **28,** 159–161.

——, and B. Kärcher, 2002: First interactive simulations of cirrus clouds formed by homogeneous freezing in the ECHAM GCM. *J. Geophys. Res.,* **107,** 4105, doi:10.1029/2001JD000767.

——, and G. Lesins, 2002: Stronger constraints on the anthropogenic indirect aerosol effect. *Science,* **298,** 1012–1016.

——, and J. Feichter, 2005: Global indirect aerosol effects: A review. *Atmos. Chem. Phys.,* **5,** 715–737.

——, ——, C. C. Chuang, and J. E. Penner, 1999: Predicting the number of cloud droplets in the ECHAM GCM. *J. Geophys. Res.,* **104,** 9169–9198.

——, ——, J. E. Penner, and W. R. Leaitch, 2000: Indirect effect of sulfate and carbonaceous aerosols: A mechanistic treatment. *J. Geophys. Res.,* **105,** 12 193–12 206.

——, J. Humble, W. R. Leaitch, G. A. Isaac, and I. Gultepe, 2001: Simulations of ice clouds during FIRE ACE using the CCCMA single column model. *J. Geophys. Res.,* **106,** 15 123–15 138.

Mason, B. J., and J. Maybank, 1958: Ice-nucleating properties of some natural mineral dusts. *Quart. J. Roy. Meteor. Soc.,* **84,** 235–241.

Menon, S., A. D. DelGenio, D. Koch, and G. Tselioudis, 2002: GCM simulations of the aerosol indirect effect: Sensitivity to cloud parameterization and aerosol burden. *J. Atmos. Sci.,* **59,** 692–713.

Pitter, R. L., and H. R. Pruppacher, 1973: A wind tunnel investigation of freezing of small water drops falling at terminal velocity in air. *Quart. J. Roy. Meteor. Soc.,* **99,** 540–550.

Pruppacher, H. R., and J. D. Klett, 1997: *Microphysics of Clouds and Precipitation.* Kluwer Academic, 954 pp.

Ramanathan, V., P. J. Crutzen, J. T. Kiehl, and D. Rosenfeld, 2001: Aerosols, climate and the hydrological cycle. *Science,* **294,** 2119–2124.

Ramaswamy, V., and Coauthors, 2001: Radiative forcing of climate change. *Climate Change 2001: The Scientific Basis,* J. T. Houghton et al., Eds., Cambridge University Press, 349–416.

Roeckner, E., and Coauthors, 1996: The atmospheric general circulation model ECHAM4: Model description and simulation of the present day climate. Tech. Rep. 218, Max-Planck Institute for Meteorology, Hamburg, Germany, 90 pp.

Rogers, R. R., and M. K. Yau, 1989: *A Short Course in Cloud Physics.* Pergamon, 293 pp.

Sassen, K., P. J. DeMott, J. M. Prospero, and M. R. Poellot, 2003: Saharan dust storms and indirect aerosol effects on clouds: CRYSTAL-FACE results. *Geophys. Res. Lett.,* **30,** 1633, doi:10.1029/2003GL017371.

Schaller, R. C., and N. Fukuta, 1979: Ice nucleation by aerosol-particles—experimental studies using a wedge-shaped ice thermal-diffusion chamber. *J. Atmos. Sci.,* **36,** 1788–1802.

Schnell, R. C., and G. Vali, 1976: Biogenic ice nuclei. Part I: Terrestrial and marine sources. *J. Atmos. Sci.,* **33,** 1554–1564.

Schütz, L., and M. Sebert, 1987: Mineral aerosols and source identification. *J. Aerosol Sci.,* **18,** 1–10.

Sokolik, I., and B. Toon, 1999: Incorporation of mineralogical composition into models of the radiative properties of mineral aerosol from UV to IR wavelengths. *J. Geophys. Res.,* **104,** 9423–9444.

Stendel, M., and K. Arpe, 1997. Evaluation of the hydrological cycle in reanalysis and observations. Tech. Rep. 228, Max-Planck Institute for Meteorology, Hamburg, Germany, 52 pp.

Usher, C. R., A. E. Michel, and V. H. Grassian, 2003: Reactions on mineral dust. *Chem. Rev.,* **103,** 4883–4939.

Wentz, F. J., 1997: A well-calibrated ocean algorithm for SSM/I. *J. Geophys. Res.,* **102,** 8703–8718.

Wielicki, B. A., and Coauthors, 2002: Evidence for large decadal variability in the tropical mean radiative energy budget. *Science,* **295,** 841–844.

Yankofsky, S. A., Z. Levin, T. Bertold, and N. Sandlerman, 1981: Some basic characteristics of bacterial freezing nuclei. *J. Appl. Meteor.,* **20,** 1013–1019.

Young, K. C., 1974: A numerical simulation of wintertime, orographic precipitation. Part 1: Description of model microphysics and numerical technique. *J. Atmos. Sci.,* **31,** 1735–1748.

Zuberi, B., A. K. Bertram, C. A. Cassa, L. T. Molina, and M. J. Molina, 2002: Heterogeneous nucleation of ice in (NH4)2SO4-H2O particles with mineral dust immersions. *Geophys. Res. Lett.,* **29,** 1504, doi:10.1029/2001GL014289.